

Cross-Layer Federated Learning Optimization in MIMO Networks

Sihua Wang, *Student Member, IEEE*, Mingzhe Chen, *Member, IEEE*,
 Cong Shen, *Senior Member, IEEE*, Changchuan Yin, *Senior Member, IEEE*,
 and Christopher G. Brinton, *Senior Member, IEEE*

Abstract

In this paper, the performance optimization of federated learning (FL), when deployed over a realistic wireless multiple-input multiple-output (MIMO) communication system with digital modulation and over-the-air computation (AirComp) is studied. In particular, an MIMO system is considered in which edge devices transmit their local FL models (trained using their locally collected data) to a parameter server (PS) using beamforming to maximize the number of devices scheduled for transmission. The PS, acting as a central controller, generates a global FL model using the received local FL models and broadcasts it back to all devices. Due to the limited bandwidth in a wireless network, AirComp is adopted to enable efficient wireless data aggregation. However, fading of wireless channels can produce aggregate distortions in an AirComp-based FL scheme. To tackle this challenge, we propose a modified federated averaging (FedAvg) algorithm that combines digital modulation with AirComp to mitigate wireless fading while ensuring the communication efficiency. This is achieved by a joint transmit and receive beamforming design, which is formulated as a optimization problem to dynamically adjust the beamforming matrices based on current FL model parameters so as to minimize the transmitting error and ensure the FL performance. To achieve this goal, we first analytically characterize how the beamforming matrices affect the performance of the FedAvg in different iterations. Based on this relationship, an artificial neural network (ANN) is used to estimate the local FL models of all devices and adjust the beamforming matrices at the PS for future model transmission. The algorithmic advantages and improved performance of the proposed methodologies are demonstrated through extensive numerical experiments.

S. Wang and C. Yin are with the Beijing Laboratory of Advanced Information Network, and the Beijing Key Laboratory of Network System Architecture and Convergence, Beijing University of Posts and Telecommunications, Beijing 100876, China. Emails: sihuawang@bupt.edu.cn; ccyin@ieee.org.

M. Chen is with the Department of Electrical and Computer Engineering, Princeton University, Princeton, NJ, 08544, USA, Email: mingzhe@princeton.edu.

Cong Shen is with the Charles L. Brown Department of Electrical and Computer Engineering, University of Virginia, Charlottesville, VA, USA, Email: cong@virginia.edu.

Christopher G. Brinton is with the School of Electrical and Computer Engineering, Purdue University, West Lafayette, IN, USA, Email: cgb@purdue.edu.

Index Terms

Federated learning, MIMO, AirComp, digital modulation.

I. INTRODUCTION

Federated learning (FL) has been extensively studied as a distributed machine learning approach with data privacy [1]–[5]. During the FL training process, edge devices are required to train a local learning model using its collected data and transmit the trained learning model to a parameter server (PS) for global model aggregation. The PS, acting as a central center, can coordinate the process across edge devices and broadcast the global model to all devices. This procedure is repeated across several rounds until achieving an acceptable accuracy of the trained model.

Since the PS and edge devices must exchange their trained models iteratively over the wireless channels, FL performance can be significantly affected by imperfect and dynamic wireless transmission in both uplink and downlink. Compared to the PS broadcasting FL models to edge devices, edge devices uploading local models to the PS is more challenging due to their limited transmit power [6]–[10]. To tackle this challenge, over-the-air computation (also known as AirComp) techniques have recently been integrated into the implementation of FL [11]–[15]. Instead of decoding the individual local models of each device and then aggregating, AirComp allows edge devices to transmit their model parameters simultaneously over the same radio resources and decoding the average model (global model) directly at the PS [16]–[18]. However, most of these existing works, such as [19] and [20], focused on the use of AirComp for analog modulation due to its simplicity for FL convergence analysis, which may not be desirable for practical wireless communication systems that almost exclusively use digital modulations. In consequence, it is necessary to study the implementation of AirComp-based FL over digital modulation-based wireless systems.

A. Related Works

Recent works such as [21]–[27] have studied several important problems related to the implementation of AirComp-based FL over wireless networks. The authors in [21] minimized the mean-squared error (MSE) of the FL model during AirComp transmission under transmit power constraints in a multiuser multiple-input multiple-output (MIMO) system. In [22], the

authors maximized the number of devices that can participate in FL training under certain MSE requirements in an AirComp-based MIMO framework. A joint machine learning rate and receiver beamforming matrix optimization method was proposed in [23] to reduce the aggregate distortion and satisfy an FL performance requirement. The authors in [24] investigated the deployment of FL over an AirComp-based wireless network to minimize the energy consumption of edge devices. In [25], the authors optimized the set of participating devices in an AirComp-assisted FL framework to speed up FL convergence. A receive beamforming scheme was designed in [26] to optimize FL performance without knowing channel state information. The authors in [27] minimized the FL model aggregation error under a channel alignment constraint in an MIMO system. However, most of these existing works [21]–[27] investigated the implementation of AirComp-based FL over analog modulation-based wireless systems, which may not be directly applied for practical digital modulation based wireless systems since these works do not consider coding and digital modulation.

Recently, several works [28]–[33] have studied the implementation of AirComp FL over digital modulation based wireless systems. The authors in [28] designed one-bit quantization and modulation schemes for edge devices. One-bit gradient quantization scheme is proposed in [29] to achieve fast FL model aggregation. In [30], the authors designed a joint channel decoding and aggregation decoding schemes based on binary phase shift keying (BPSK) modulation for AirComp FL. The authors in [31] evaluated the performance of FL gradient quantization in digital AirComp. In [32], the convergence of FL implemented over an AirComp-based MIMO system is derived. The authors in [33] proposed a digital transmission protocol tailored to FL over wireless device-to-device networks. However, these prior works [28]–[33] mainly used low order digital modulation (i.e., BPSK) and hence their designed AirComp FL cannot be easily extended to modern wireless systems that use high-order digital modulation schemes such as quadrature amplitude modulation (QAM). This is because the transmitted symbols that are processed by low order digital modulation (such as the symbols -1 and $+1$ in BPSK) are linearly superimposed. This linear superimposition does not exist in the high-order digital modulation schemes with complex mapping relationships between bits and symbols (such as Gray code).

B. Contributions

The main contribution of this paper is to develop a novel AirComp FL framework over high-order digital modulation-based wireless systems. Our key contributions include:

- We propose a novel AirComp-based MIMO system in which distributed wireless devices modulate their trained local FL parameters into symbols and simultaneously transmit these modulated symbols to a PS that directly generates the global FL model via its received symbols. To optimize the FL training performance in the proposed system, the PS and devices must dynamically adjust the transmit and receive beamforming matrices over unreliable wireless channels. To this end, we formulate this joint transmit and receive beamforming matrix design problem as an optimization problem whose goal is to minimize the FL training loss.
- To solve this problem, we first analytically characterize how the errors introduced by the proposed AirComp system affect FL training loss. Our analysis shows that the introduced errors caused by wireless transmission (i.e., fading and additive white Gaussian noise) and digital post-processing (i.e., digital demodulation) determine the gap between the optimal FL model that the FL targets to converge and the trained FL model. In particular, the errors caused by wireless transmission depends on the channel conditions and the trained FL model parameters. However, the errors caused by digital post-processing depend on the adopted modulation scheme and the number of devices participated in FL training. Hence, to minimize the errors caused by both wireless transmission and digital post-processing, the PS and the devices must dynamically adjust the transmit and receive beamforming matrices based on the adopted modulation scheme, the trained FL model parameters, and channel conditions.
- To find the optimal transmit and receive beamforming matrices, we first introduce an artificial neural network (ANN)-based algorithm to predict the FL model parameters of all devices since optimizing beamforming matrices requires the information of each trained local model parameters which cannot be obtained by the PS. Then, given the predicted parameters, we derive a closed-form solution of the optimal transmit and receive beamforming matrices based on the adopted modulation scheme and channel conditions that minimizes the distance between the received signals of all devices and the predicted parameters in the decision region, which ensures the accuracy for model aggregation and FL performance.
- Numerical evaluation results on real-world machine learning task datasets show that our proposed AirComp-based system can improve the identification accuracy by up to 20.5% and 10.5% compared to the AirComp-based system with analog modulation and BPSK, respectively.

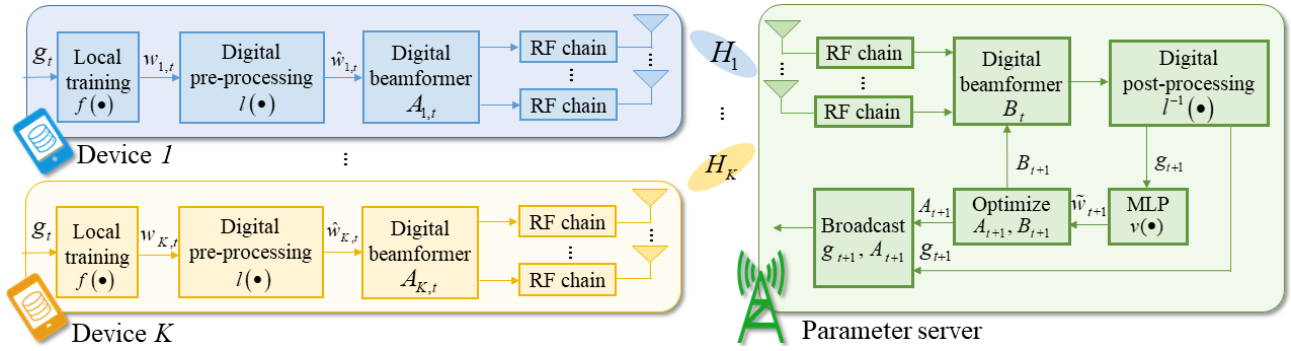


Fig. 1. The structure of a FL algorithm deployed over multiple devices and one PS in a MIMO communication system.

TABLE I
LIST OF NOTATIONS

Notation	Description	Notation	Description
K	Number of devices	M	Adopted modulation order
N_r	Number of antennas on the PS	N_t	Number of antennas on devices
N_k	Number of training data samples on device k	$(\mathbf{x}_{k,n}, \mathbf{y}_{k,n})$	Training data sample n on device k
N	Number of training data samples of all devices	\mathbf{g}_t	Global FL model
$\mathbf{w}_{k,t}$	Local FL model	$\Delta\mathbf{w}_{k,t}$	Updates of $\mathbf{w}_{k,t}$
$\hat{\mathbf{w}}_{k,t}$	Modulated symbol vector of $\mathbf{w}_{k,t}$	$\Delta\tilde{\mathbf{w}}_{k,t}$	Prediction of $\Delta\mathbf{w}_{k,t}$
$\Delta\hat{\mathbf{w}}_{k,t}$	Modulated symbol vector of $\Delta\tilde{\mathbf{w}}_{k,t}$	\mathbf{n}_t	Additive white Gaussian noise
$\mathbf{A}_{k,t}$	Transmit beamforming matrix	\mathbf{B}_t	Receive beamforming matrix
\mathbf{H}_k	Channel vector between device k and the PS	P_0	Maximal transmit power on device
ξ	Minimum Euclidean distance in decision region	a_i^I, a_i^Q	Constellation point of symbol i
\mathbf{a}^*	Vector of predicted constellation point	\mathcal{M}	Set of all constellation points

The rest of this paper is organized as follows. The system model and problem formulation for the AirComp-based system in FL framework are described in Section II. Section III analyzes the convergence of the designed FL framework and derives a closed-form optimal design of the transmit and receive beamforming matrices based on the analysis. In Section IV, our numerical evaluation is presented and discussed. Finally, conclusions are drawn in Section V.

II. SYSTEM MODEL AND PROBLEM FORMULATION

We consider an FL system implemented over a cellular network, where K wireless edge devices train their individual machine learning models and send the machine learning parameters

to a central PS through a noisy wireless MAC as shown in Fig. 1. In the considered model, the PS is equipped with N_r antennas while each device k is equipped with N_t antennas.

Each device has N_k training data samples and each training data sample n in device k consists of an input feature vector $\mathbf{x}_{k,n} \in \mathbf{R}^{N_I \times 1}$ and a corresponding label vector $\mathbf{y}_{k,n} \in \mathbf{R}^{N_O \times 1}$ where N_I and N_O are the dimension of input and output vectors, respectively. Table I provides a summary of the notations used throughout this paper. The objective of training is to minimize the global loss function over all data samples, which is given by

$$F(\mathbf{g}) = \min_{\mathbf{g}} \frac{1}{N} \sum_{k=1}^K \sum_{n=1}^{N_k} f(\mathbf{g}, \mathbf{x}_{k,n}, \mathbf{y}_{k,n}), \quad (1)$$

where $\mathbf{g} \in \mathbf{R}^{V \times 1}$ is a vector that represents the global FL model of dimension V trained across the devices with $N = \sum_{k=1}^K N_k$ being the total number of training data samples of all devices. $f(\mathbf{g}, \mathbf{x}_{k,n}, \mathbf{y}_{k,n})$ is the local loss function of each device k with FL model \mathbf{g} and data sample $(\mathbf{x}_{k,n}, \mathbf{y}_{k,n})$.

To minimize the global loss function in (1) in a distributed manner, each device can update its FL model using its local dataset with a backward propagation (BP) algorithm based on stochastic gradient descent (SGD), which can be expressed as

$$\mathbf{w}_{k,t} = \mathbf{g}_t - \lambda \sum_{n \in \mathcal{N}_{k,t}} \frac{\partial f(\mathbf{g}, \mathbf{x}_{k,n}, \mathbf{y}_{k,n})}{\partial \mathbf{g}}, \quad (2)$$

where λ is the learning rate, $\mathcal{N}_{k,t}$ is the subset of training data samples (i.e., minibatch) selected from device k 's training dataset \mathcal{N}_k at iteration t , $\mathbf{w}_{k,t}$ is the updated local FL model of device k at iteration t .

Given $\mathbf{w}_{k,t}$, distributed devices must simultaneously exchange their model parameters with the PS via bandwidth-limited wireless fading channels for model aggregation. The equation of model aggregation is given by

$$\mathbf{g}_t = \sum_{k=1}^K \frac{|\mathcal{N}_k|}{N} \mathbf{w}_{k,t}, \quad (3)$$

where $|\mathcal{N}_k|$ represents the number of data samples in \mathcal{N}_k .

To ensure all devices can participate in FL model exchanging via wireless fading channels, each device adopts digital modulation to mitigate wireless fading and the PS adopts beamforming to maximize the number of devices scheduled for FL parameter transmission. Next, we will mathematically introduce the FL training and transmission process integrated with digital modulation in the considered MIMO communication system. In particular, we first introduce our

designed digital modulation process that consists of two steps: (i) digital pre-processing at the devices and (ii) digital post-processing at the PS.

A. Digital pre-processing at the devices

To transmit $\mathbf{w}_{k,t}$ over wireless fading channels, each device k leverages digital pre-processing to represent each numerical FL parameter in $\mathbf{w}_{k,t}$ using a symbol vector, which is given by

$$\hat{\mathbf{w}}_{k,t} = l(\mathbf{w}_{k,t}), \quad (4)$$

where $\hat{\mathbf{w}}_{k,t} \in \mathbf{R}^W$ is a modulated symbol vector with W being the number of symbols, and $l(\cdot)$ denotes the digital pre-processing function that combines decimal-to-binary conversion and digital modulation where the decimal-to-binary conversion is used to represent each numerical FL parameter with a binary coded bit-interleaved vector and the digital modulation is used to modulate several binary bits as a symbol [34]. For convenience, the modulated signal $\hat{\mathbf{w}}_{k,t}$ is normalized (i.e., $|\hat{\mathbf{w}}_{k,t}| = 1$). We use rectangular M -quadrature-amplitude modulation (QAM) for digital modulation and it can be extended to other types of digital modulation schemes.

In our model, each device sends $\hat{\mathbf{w}}_{k,t}$ to the PS at each iteration t using fully-digital beamforming with low RF complexity. Given the transmit beamforming matrix $\mathbf{A}_{k,t} \in \mathbf{C}^{N_t \times W}$ and the maximal transmit power P_0 at device k , the power constraint can be expressed as

$$\mathbb{E}(|\mathbf{A}_{k,t} \hat{\mathbf{w}}_{k,t}|^2) = |\mathbf{A}_{k,t}|^2 \leq P_0. \quad (5)$$

where $\mathbb{E}(x)$ represents the expectation of x .

B. Post-processing at the PS

Considering the multiple access channel property of wireless communication, the received signal at the PS is given by

$$\mathbf{s}_t(\mathbf{A}_t) = \sum_{k=1}^K \mathbf{H}_k \mathbf{A}_{k,t} \hat{\mathbf{w}}_{k,t} + \mathbf{n}_t \quad (6)$$

where $\mathbf{A}_t = [\mathbf{A}_{1,t}, \dots, \mathbf{A}_{K,t}]$ denotes the transmit beamforming matrices of all devices, $\mathbf{H}_k \in \mathbf{C}^{N_r \times N_t}$ denotes the MIMO channel vector for the link from device k to the PS, and $\mathbf{n}_t \in \mathbf{C}^{N_r}$ denotes additive white Gaussian noise. The entries of \mathbf{H}_k and \mathbf{n}_t are assumed to be independent and identically distributed (i.i.d.) complex Gaussian variables with zero mean.

Since $\mathbf{s}_t(\mathbf{A}_t)$ is the weighted sum of all users' local FL models, we consider directly generating the global FL model \mathbf{g}_{t+1} from $\mathbf{s}_t(\mathbf{A}_t)$. This is a major difference between the existing works and this work. The digital beamformer output signal can be expressed as

$$\hat{\mathbf{s}}_t(\mathbf{B}_t, \mathbf{A}_t) = \mathbf{B}_t^H \mathbf{s}_t(\mathbf{A}_t), \quad (7)$$

where $\mathbf{B}_t \in \mathbf{C}^{N_r \times W}$ is the digital receive beamforming matrix.

Given the received symbol vector $\hat{\mathbf{s}}_t(\mathbf{B}_t, \mathbf{A}_t)$, the PS can reconstruct the numerical parameters in global FL model \mathbf{g}_{t+1} , which can be expressed as

$$\mathbf{g}_{t+1}(\mathbf{B}_t, \mathbf{A}_t) = l^{-1}(\hat{\mathbf{s}}_t(\mathbf{B}_t, \mathbf{A}_t)), \quad (8)$$

where $l^{-1}(\cdot)$ is the inverse function with respect to $l(\cdot)$ that combines the binary-to-decimal function and the digital demodulation function.

C. Problem Formulation

Next, we introduce our optimization problem. Our goal is to minimize the FL training loss by designing the transmit and receive beamforming matrices under the total transmit power constraint of each device, which is formulated as follows:

$$\min_{\mathbf{B}, \mathbf{A}} F(\mathbf{g}(\mathbf{B}_T, \mathbf{A}_T)), \quad (9)$$

$$\text{s.t. } |\mathbf{A}_{k,t}|^2 \leq P_0, \forall k \in \mathcal{K}, \forall t \in \mathcal{T}. \quad (9a)$$

where $\mathbf{A} = [\mathbf{A}_1, \dots, \mathbf{A}_T]$ and $\mathbf{B} = [\mathbf{B}_1, \dots, \mathbf{B}_T]$ are the transmit and receive beamforming matrices for all iterations, respectively. T is a constant which is large enough to guarantee the convergence of FL.

From (9), we can see that the FL training loss $F(\mathbf{g}(\mathbf{B}_T, \mathbf{A}_T))$ depends on the global FL model $\mathbf{g}(\mathbf{B}_T, \mathbf{A}_T)$ that is trained iteratively. Meanwhile, as shown in (6) and (7), edge devices and the PS must dynamically adjust \mathbf{A}_t and \mathbf{B}_t based on current FL model parameters to minimize the gradient deviation caused by AirComp in the considered MIMO system with digital modulation. However, the PS does not know the gradient vector of each edge device and hence the PS cannot proactively adjust the receive beamforming matrix using traditional optimization algorithms. To tackle this challenge, we propose an ANN-based algorithm that enables the PS to predict the local FL gradient parameters of each device. Based on the predicted local FL model parameters, the PS and edge devices can cooperatively optimize the beamforming matrices to improve the

performance of FL. Next, we first mathematically analyze the FL update process in the considered AirComp-based system to capture the relationship between the beamforming matrix design and the FL training loss per iteration. Based on this relationship, we then derive the closed-form solution of optimal \mathbf{A}_t and \mathbf{B}_t that depends on the predicted FL models achieved by an ANN-based algorithm.

III. SOLUTION FOR PROBLEM (9)

To solve (9), we first analyze the convergence of the considered FL so as to find the relationship between digital beamforming matrices \mathbf{A}_t , \mathbf{B}_t , and FL training loss in (9). The analytical result shows that the optimization of beamforming matrices \mathbf{A}_t and \mathbf{B}_t depends on the FL parameters transmitted by each device. However, the PS does not know these FL parameters since it must determine the beamforming matrices \mathbf{A}_t and \mathbf{B}_t before the FL parameter transmission. Therefore, we propose to use neural networks to predict the local FL models of each device and proactively determine the beamforming matrices using these predicted FL parameters.

A. Analysis of the Convergence of the Designed FL

We first analyze the convergence of the considered FL system. Since the update of the global FL model depends on the instantaneous signal-to-interference-plus-noise ratio (SINR) affected by the digital beamforming matrices \mathbf{A}_t and \mathbf{B}_t , we can analyze only the expected convergence rate of FL. To analyze the expected convergence rate of FL, we first assume that a) the loss function $F(\mathbf{g})$ is L -smooth with the Lipschitz constant $L > 0$, b) $F(\mathbf{g})$ is strongly convex with positive parameter μ , c) $F(\mathbf{g})$ is twice-continuously differentiable, and d) $\|\nabla f(\mathbf{g}_t, \mathbf{x}_{kn}, \mathbf{y}_{kn})\|^2 \leq \zeta_1 + \zeta_2 \|\nabla F(\mathbf{g}_t)\|^2$, as done in [35]. These assumptions can be satisfied by several widely used loss functions such as mean squared error, logistic regression, and cross entropy. Based on these assumptions, next, we first derive the upper bound of the FL training loss at one FL training step. The expected convergence rate of the designed FL algorithm can now be obtained by the following theorem.

Theorem 1. Given the optimal global FL model \mathbf{g}^* , the current global FL model \mathbf{g}_t , the transmit beamforming matrix \mathbf{A}_t , and the receive beamforming matrix \mathbf{B}_t , $\mathbb{E}(F(\mathbf{g}_{t+1}(\mathbf{A}_t, \mathbf{B}_t)) - F(\mathbf{g}^*))$

can be upper bounded as

$$\begin{aligned} \mathbb{E}(F(\mathbf{g}_{t+1}(\mathbf{A}_t, \mathbf{B}_t)) - F(\mathbf{g}^*)) &\leq \mathbb{E}(F(\mathbf{g}_t) - F(\mathbf{g}^*)) \\ &\quad - \frac{1}{2L} \|\nabla F(\mathbf{g}_t)\|^2 + \frac{1}{2L} \mathbb{E}(\|\mathbf{e}_t\| + \|\hat{\mathbf{e}}_t(\mathbf{A}_t, \mathbf{B}_t)\|)^2, \end{aligned} \quad (10)$$

where

$$\mathbf{e}_t = \frac{\sum_{k=1}^K \sum_{n \in \mathcal{N}_{k,t}} \nabla f(\mathbf{g}_t, \mathbf{x}_{n,k}, \mathbf{y}_{n,k})}{\sum_{k=1}^K |\mathcal{N}_{k,t}|} - l^{-1} \left(\frac{\sum_{k=1}^K l \left(\sum_{n \in \mathcal{N}_{k,t}} \nabla f(\mathbf{g}_t, \mathbf{x}_{n,k}, \mathbf{y}_{n,k}) \right)}{\sum_{k=1}^K |\mathcal{N}_{k,t}|} \right) \quad (11)$$

with the first term being the gradient trained by SGD and the second term being the gradient demodulated from a sum of all selected devices' symbols (i.e., $\frac{\sum_{k=1}^K l \left(\sum_{n \in \mathcal{N}_{k,t}} \nabla f(\mathbf{g}_t, \mathbf{x}_{n,k}, \mathbf{y}_{n,k}) \right)}{\sum_{k=1}^K |\mathcal{N}_{k,t}|}$), and

$$\begin{aligned} \hat{\mathbf{e}}_t(\mathbf{A}_t, \mathbf{B}_t) &= l^{-1} \left(\frac{\sum_{k=1}^K l \left(\sum_{n \in \mathcal{N}_{k,t}} \nabla f(\mathbf{g}_t, \mathbf{x}_{n,k}, \mathbf{y}_{n,k}) \right)}{\sum_{k=1}^K |\mathcal{N}_{k,t}|} \right) \\ &\quad - l^{-1} \left(\frac{\mathbf{B}_t \left(\sum_{k=1}^K \mathbf{H}_k \mathbf{A}_{k,t} l \left(\sum_{n \in \mathcal{N}_{k,t}} \nabla f(\mathbf{g}_t, \mathbf{x}_{n,k}, \mathbf{y}_{n,k}) \right) + \mathbf{n}_t \right)}{\sum_{k=1}^K |\mathcal{N}_{k,t}|} \right). \end{aligned} \quad (12)$$

Proof: See Appendix A. ■

From Theorem 1, we see that, since \mathbf{e}_t does not depend on \mathbf{A}_t or \mathbf{B}_t , the optimization of the digital beamforming matrices cannot minimize \mathbf{e}_t . In consequence, we can only minimize $\|\hat{\mathbf{e}}_t\|$ to decrease the gap between the FL training loss at iteration $t+1$ and the optimal FL training loss (i.e., $\mathbb{E}(F(\mathbf{g}_{t+1}) - F(\mathbf{g}^*))$). Thus, problem (9) can be rewritten as

$$\min_{\mathbf{B}_t, \mathbf{A}_t} \|\hat{\mathbf{e}}_t\|^2 \quad (13)$$

$$\text{s.t. } |\mathbf{A}_{k,t}|^2 \leq P_0, \forall k \in \mathcal{K}, \forall t \in \mathcal{T}. \quad (13a)$$

To minimize $\|\hat{\mathbf{e}}_t\|$ in (13), the PS and edge devices must obtain the information of MIMO channel vector \mathbf{H}_k as well as the trained gradients $l \left(\sum_{n \in \mathcal{N}_{k,t}} \nabla f(\mathbf{g}_t, \mathbf{x}_{n,k}, \mathbf{y}_{n,k}) \right)$ so as to adjust \mathbf{A}_t and \mathbf{B}_t . However, the trained FL gradients $\Delta \mathbf{w}_{k,t} = \sum_{n \in \mathcal{N}_{k,t}} \nabla f(\mathbf{g}_t, \mathbf{x}_{n,k}, \mathbf{y}_{n,k})$ cannot be obtained by the PS before edge devices sending FL model parameters. Hence, the PS must predict $\Delta \mathbf{w}_{k,t}$ for optimizing \mathbf{A}_t and \mathbf{B}_t and minimizing $\|\hat{\mathbf{e}}_t\|$.

B. Prediction of the Local FL Models

Next, we explain the use of neural networks to predict the local FL model updates of all devices. Since finding a relationship among each device's local FL model updates at different iterations is a regression task and the fully-connected multilayer perceptrons (MLPs) in ANNs are good at such tasks, we propose to use MLPs instead of other neural networks such as recurrent neural networks (RNN) [36]. Next, we first explain the components of the proposed ANN-based algorithm. Then, the details to implement this algorithm for predicting each local FL model update are presented.

The proposed MLP-based prediction algorithm consists of three components: a) input, b) a single hidden layer, and c) output, which are defined as follows:

- *Input:* The input of the MLP that is implemented by the PS for predicting device k 's local FL model is a vector \mathbf{g}_{t-1} . As we mentioned in (6), all devices are able to connect with the PS so as to provide the input information for the MLP to predict the local FL models for next iteration.
- *Output:* The output of the MLP is a vector $\Delta\tilde{\mathbf{w}}_{k,t}$ that represents device k 's local FL model update at current iteration t . Based on the predicted $\Delta\tilde{\mathbf{w}}_{k,t}$, the PS can adjust the transmit and receive beamforming matrices proactively to minimize problem (16).
- *A Single Hidden Layer:* The hidden layer of a MLP is used to learn the nonlinear relationships between input vector \mathbf{g}_{t-1} and the output vector $\Delta\tilde{\mathbf{w}}_{k,t}$. The weight matrix that represents the connection strength between the input vector and the neurons in the hidden layer is $\mathbf{v}^{\text{in}} \in \mathbf{C}^{D \times V}$ where D is the number of neurons in the single hidden layer. Meanwhile, the weight matrix that captures the strengths of the connections between the neurons in the hidden layer and the output vector is $\mathbf{v}^{\text{out}} \in \mathbf{C}^{V \times D}$.

Having the components of the MLP, next, we introduce the use of the MLP to predict each device's local FL model update. The states of the neurons in the hidden layer are given by

$$\mathbf{v} = \sigma(\mathbf{v}^{\text{in}} \mathbf{g}_{k,t-1} + \mathbf{b}_v), \quad (14)$$

where $\sigma(x) = \frac{2}{1+\exp(-2x)} - 1$ and $\mathbf{b}_v \in \mathbf{C}^{D \times 1}$ is the bias. Then, the output of the MLP can be given by

$$\Delta\tilde{\mathbf{w}}_{k,t} = \mathbf{v}^{\text{out}} \mathbf{v} + \mathbf{b}_o, \quad (15)$$

where $\mathbf{b}_o \in \mathbf{C}^{V \times 1}$ is a vector of bias.

To predict each device's local FL model update, the MLP must be trained by an online gradient descent method. However, in the considered model, the PS can only obtain \mathbf{g}_t that is directly demodulated from the received signal from all devices. Hence, the PS and the devices must exchange information to train the MLP cooperatively. In particular, at each iteration, device k first generates $\mathbf{w}_{k,t}$ using its local dataset and \mathbf{g}_{t-1} received from the PS. Then, device k calculates the training loss of MLP and transmits it to the PS. Based on the value of the training loss, the PS and device k can update its MLP synchronously. Since each device only needs to transmit its training loss, the cost for information exchange can be ignored compared with the communicated DNN model weights.

C. Optimization of the Beamforming Matrices

Having the predicted local FL model updates $\Delta\tilde{\mathbf{w}}_{k,t}$, the PS can optimize the beamforming matrices \mathbf{A}_t and \mathbf{B}_t to solve Problem (13). Substituting $\Delta\tilde{\mathbf{w}}_{k,t}$, (6), and (7) into (13), we have

$$\min_{\mathbf{B}_t, \mathbf{A}_t} \left\| l^{-1} \left(\frac{\sum_{k=1}^K l(\Delta\tilde{\mathbf{w}}_{k,t})}{\sum_{k=1}^K |\mathcal{N}_{k,t}|} \right) - l^{-1} \left(\frac{\mathbf{B}_t \left(\sum_{k=1}^K \mathbf{H}_k \mathbf{A}_{k,t} l(\Delta\tilde{\mathbf{w}}_{k,t}) + \mathbf{n}_t \right)}{\sum_{k=1}^K |\mathcal{N}_{k,t}|} \right) \right\|^2 \quad (16)$$

$$\text{s.t. } |\mathbf{A}_{k,t}|^2 \leq P_0, \forall k \in \mathcal{K}, \forall t \in \mathcal{T}. \quad (16a)$$

In (16), $l^{-1} \left(\frac{\sum_{k=1}^K l(\Delta\tilde{\mathbf{w}}_{k,t})}{\sum_{k=1}^K |\mathcal{N}_{k,t}|} \right)$ is independent of \mathbf{A}_t and \mathbf{B}_t and can be regarded as a constant. However, the existence of the inverse function $l^{-1}(\cdot)$ defined in (8) significantly increases the complexity for solving (16). Considering $l^{-1}(\cdot)$ that is used to demodulate the symbols into numerical FL parameters, the minimization of the gap between $l^{-1} \left(\frac{\sum_{k=1}^K l(\Delta\tilde{\mathbf{w}}_{k,t})}{\sum_{k=1}^K |\mathcal{N}_{k,t}|} \right)$ and $l^{-1} \left(\frac{\mathbf{B}_t \left(\sum_{k=1}^K \mathbf{H}_k \mathbf{A}_{k,t} l(\Delta\tilde{\mathbf{w}}_{k,t}) + \mathbf{n}_t \right)}{\sum_{k=1}^K |\mathcal{N}_{k,t}|} \right)$ is equivalent to minimize the distance between $\frac{\sum_{k=1}^K l(\Delta\tilde{\mathbf{w}}_{k,t})}{\sum_{k=1}^K |\mathcal{N}_{k,t}|}$ and $\frac{\mathbf{B}_t \left(\sum_{k=1}^K \mathbf{H}_k \mathbf{A}_{k,t} l(\Delta\tilde{\mathbf{w}}_{k,t}) + \mathbf{n}_t \right)}{\sum_{k=1}^K |\mathcal{N}_{k,t}|}$ in the decision region of digital demodulation, as shown in Fig. 2. To this end, in this section, we first derive the position of $\frac{\sum_{k=1}^K l(\Delta\tilde{\mathbf{w}}_{k,t})}{\sum_{k=1}^K |\mathcal{N}_{k,t}|}$ in the decision region and remove $l^{-1}(\cdot)$ from (16) for simplification. Then, we present a closed-form optimal design of the transmit and receive beamforming matrices.

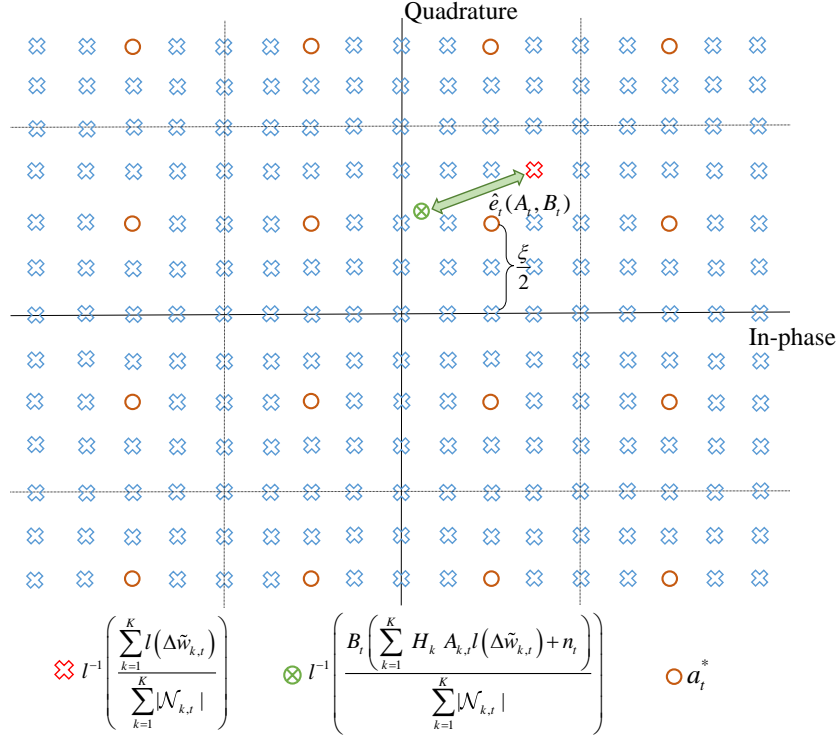


Fig. 2. An example of 16-QAM constellation at the PS with 4 devices.

Given $\Delta \tilde{w}_{k,t}$ and the digital pre-processing function $l(\cdot)$ defined in (4), the modulated symbol vector $\Delta \hat{w}_{k,t} = l(\Delta \tilde{w}_{k,t}) = [\Delta \hat{w}_{k,t,1}^I \Delta \hat{w}_{k,t,1}^Q, \dots, \Delta \hat{w}_{k,t,L}^I \Delta \hat{w}_{k,t,L}^Q]$ can be obtained where $\Delta \hat{w}_{k,t,i}^I$ and $\Delta \hat{w}_{k,t,i}^Q$ are the i -th in-phase and quadrature symbols modulated by $\Delta \tilde{w}_{k,t}$, respectively. Since in-phase and quadrature-phase symbols that have vertical and horizontal decision regions are mutually independent, the value of $l^{-1} \left(\frac{\sum_{k=1}^K \Delta \hat{w}_{k,t}}{\sum_{k=1}^K |\mathcal{N}_{k,t}|} \right)$ can be obtained via individually analyzing the decision region of each in-phase and quadrature-phase symbols which are

$$\left| \frac{1}{\sum_{k=1}^K |\mathcal{N}_{k,t}|} \sum_{k=1}^K \Delta \hat{w}_{k,t,i}^I - a_i^I \right| \leq \frac{\xi}{2}, \quad \left| \frac{1}{\sum_{k=1}^K |\mathcal{N}_{k,t}|} \sum_{k=1}^K \Delta \hat{w}_{k,t,i}^Q - a_i^Q \right| \leq \frac{\xi}{2}, \quad (17)$$

where $a_i^I, a_i^Q \in \mathcal{M} = \left\{ \frac{1-\sqrt{M}}{2}\xi, \frac{3-\sqrt{M}}{2}\xi, \dots, \frac{\sqrt{M}-3}{2}\xi, \frac{\sqrt{M}-1}{2}\xi \right\}$ are the constellation points in the decision region with \mathcal{M} being the set of all constellation points. $\xi = \sqrt{\frac{4P_0}{(\sqrt{M}-1)^2}}$ is the minimum Euclidean distance between two constellation points. Using (17), a_i^I and a_i^Q are given by

$$a_{t,i}^I = \left\{ x \in \mathcal{M} : -\frac{\xi}{2} + \frac{\sum_{k=1}^K \Delta \hat{w}_{k,t,i}^I}{\sum_{k=1}^K |\mathcal{N}_{k,t}|} \leq x \leq \frac{\xi}{2} + \frac{\sum_{k=1}^K \Delta \hat{w}_{k,t,i}^I}{\sum_{k=1}^K |\mathcal{N}_{k,t}|} \cap \mathcal{M} \right\} \quad (18)$$

and

$$a_{t,i}^Q = \left\{ x \in \mathcal{M} : -\frac{\xi}{2} + \frac{\sum_{k=1}^K \Delta \hat{w}_{k,t,i}^Q}{\sum_{k=1}^K |\mathcal{N}_{k,t}|} \leq x \leq \frac{\xi}{2} + \frac{\sum_{k=1}^K \Delta \hat{w}_{k,t,i}^Q}{\sum_{k=1}^K |\mathcal{N}_{k,t}|} \cap \mathcal{M} \right\}. \quad (19)$$

Given $\mathbf{a}_t^* = [a_{t,1}^I a_{t,1}^Q, \dots, a_{t,W}^I a_{t,W}^Q]$, problem (16) can be rewritten as

$$\min_{\mathbf{B}_t, \mathbf{A}_t} \left\| \mathbf{a}_t^* - \mathbf{B}_t^H \sum_{k=1}^K \mathbf{H}_k \mathbf{A}_{k,t} \Delta \hat{w}_{k,t} - \mathbf{B}_t^H \mathbf{n}_t \right\|^2 \quad (20)$$

$$\text{s.t. } \|\mathbf{A}_{k,t}\|^2 \leq P_0, \forall k \in \mathcal{K}, \forall t \in \mathcal{T}. \quad (20a)$$

where $\Delta \hat{w}_{k,t} = l(\Delta \tilde{w}_{k,t})$ is a modulated symbol vector of $\Delta \tilde{w}_{k,t}$. Problem (20) can be solved by an iterative optimization algorithm. In particular, to solve problem (20), we first fix \mathbf{B}_t , then the objective functions and constraints with respect to \mathbf{A}_t are convex and can be optimally solved by using a dual method [37]. Similarly, given \mathbf{A}_t , problem (20) is minimized as $\mathbf{B}_t^* = \left(\frac{a_t^*}{\sum_{k=1}^K \mathbf{H}_k \mathbf{A}_{k,t}^* \Delta \hat{w}_{k,t}} \right)^H$.

D. Implementation and Complexity

Next, we introduce the implementation and complexity of the designed FL algorithm. With regards to the implementation of the proposed algorithm, the PS must a) use MLPs to predict the devices' local FL models and b) design the transmit and receive beamforming matrices based on the predicted models. To train the MLPs that are used for the predictions of devices' local FL models, the PS will use the global FL model \mathbf{g}_{t-1} that is directly reconstructed from the received symbol vector $\hat{\mathbf{s}}_{t-1}$ at iteration $t-1$. Since $\hat{\mathbf{s}}_{t-1}$ that is transmitted from all devices via AirComp is originally used for the update of the global FL model, the PS does not require any additional information for training MLPs. To design the optimal transmit and receive beamforming matrices, the PS requires the maximal transmit power P_0 and the MIMO channel vector \mathbf{H}_k of each device k . Since P_0 is a fixed scalar, the data size of which is much smaller than the data size of the local FL models that the devices must transmit to the PS during each iteration. In consequence, we can ignore the overhead of each device transmitting P_0 to the PS. With regards to \mathbf{H}_k , the PS can use channel estimation methods to learn \mathbf{H}_k over each uplink channel so as to design optimal transmit and receive beamforming matrices.

Algorithm 1 Proposed FL Over AirComp-based System

- 1: **Init:** Global FL model \mathbf{g}_0 , beamforming metrics \mathbf{A}_0 and \mathbf{B}_0 , MIMO channel matrix \mathbf{H} .
- 2: **for** iterations $t = 0, 1, \dots, T$ **do**
- 3: **for** $k \in \{1, 2, \dots, K\}$ in parallel over K devices **do**
- 4: Each device calculates and returns $\mathbf{w}_{k,t}$ based on local dataset and \mathbf{g}_t in (2).
- 5: Each device leverages digital pre-processing to modulate each model parameter into a symbol.
- 6: Each device sends the symbol vector $\hat{\mathbf{w}}_{n,k}$ to the PS using the optimized transmit beamforming matrix $\mathbf{A}_{k,t}$.
- 7: **end for**
- 8: The PS directly demodulates the global FL model \mathbf{g}_{t+1} from the received superpositioned signal using (8).
- 9: The PS predicts the local FL model $\hat{\mathbf{w}}_{k,t+1}$ of each device based on demodulated \mathbf{g}_{t+1} using trained ANNs.
- 10: The PS proactively adjusts the transmit and receive beamforming matrices using the augmented Lagrangian method and broadcast the transmit beamforming matrix $\mathbf{A}_{k,t+1}$ to each device k .
- 11: **end for**

The complexity of the proposed algorithm lies in the design of the beamforming matrices. We ignore the overhead for training MLPs since we only need to train MLP once for the entire FL training process. Meanwhile, the PS has enough computational resource for training MLPs [38]. Hence, we only analyze the complexity of a dual method that is used to optimize \mathbf{A}_t and \mathbf{B}_t which has to be done for each iteration and thus the complexity scales lies in the number of iterations required to converge. For finding optimal \mathbf{A}_t and \mathbf{B}_t , problem (20) can be solved by a traditional augmented Lagrangian method that approaches the optimal solution via alternating updating \mathbf{A}_t , \mathbf{B}_t , and the Lagrangian multiplier vector. Obviously, the introduced Lagrangian multiplier vector consists of K constraints where K is the number of devices in the considered FL framework. Hence, the PS is required to sequentially update K Lagrangian multipliers, $\mathbf{A}_t = [\mathbf{A}_{1,t}, \dots, \mathbf{A}_{K,t}]$, and \mathbf{B}_t at each iteration. Let L_O be the number of iterations until the traditional augmented Lagrangian method converges, the complexity is $\mathcal{O}(L_O K^2)$.

TABLE II
SIMULATION PARAMETERS

Parameters	Values	Parameters	Values	Parameters	Values
K	20	M	64	n_t	-50 dBW
N_r	2	N_t	2	N_k	2000
P_0	0.001 W	T	50	W	7840
N_I	28	N_O	10	λ	0.01
r	1500	D	128	L_0	100

IV. SIMULATION RESULTS AND ANALYSIS

We consider a circular network area having a radius $r = 1500$ m with one PS at its center serving $K = 20$ uniformly distributed devices. In particular, the PS allocates 56 subcarriers to all devices and the bandwidth of each subcarrier is 15 kHz. The channels between the PS and devices are modeled as the independent and identically distributed Rayleigh fading channels. The other parameters used in simulations are listed in Table II. All statistical results are averaged over 5,000 independent runs. For comparison purposes, we consider three baselines: a) the proposed FL algorithm implemented over noiseless wireless channels, b) an FL algorithm that uses digital beamforming and analog modulation for FL parameter transmission [25], and c) an FL algorithm that uses digital beamforming and BPSK for FL parameter transmission [30].

To evaluate the performance of the proposed FL, MNIST dataset [39] and Fashion-MNIST dataset [40] are used. In particular, for MNIST dataset, we adopt a fully-connected neural network (FNN) that consists of two full-connection layers with 7840 ($=28 \times 28 \times 10$) model parameters. And for fashion-MNIST dataset, we adopt a FNN that consists of four full-connection layers with 83900 ($= 28 \times 28 \times 100 + 100 \times 50 + 50 \times 10$) model parameters. Each device collects 2000 data samples for training the adopted FNNs and the PS uses one MLP that consists of three layers to predict the FL gradient vector of each device. We assume that all local datasets are independent and identically distributed across the devices. All FL algorithms are considered to have converged when the value of the FL loss variance calculated over 20 consecutive iterations is less than 0.001.

A. Convergence Speed Comparisons

Fig. 3 shows how the identification accuracy of all considered algorithms changes as the number of iterations varies. From Fig. 3, we can see that the proposed AirComp method

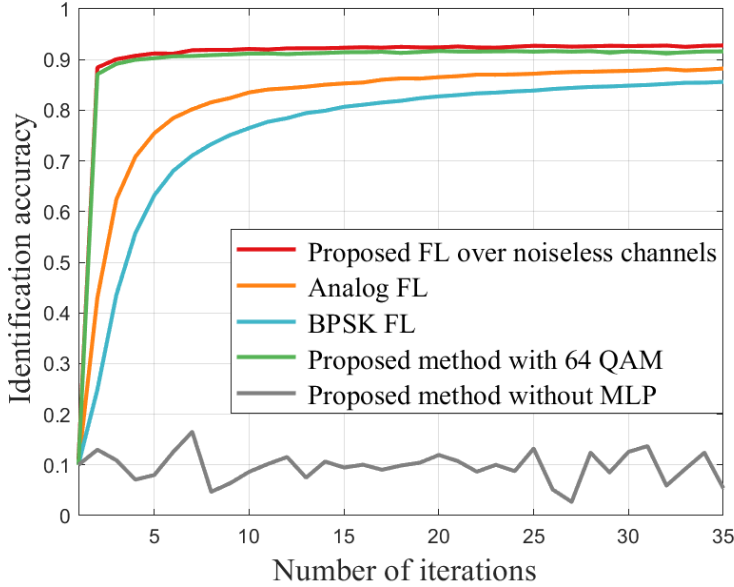


Fig. 3. Identification accuracy vs. number of iterations on MNIST dataset.

converges much faster compared to analog FL and BPSK FL. In particular, the proposed method can improve FL convergence speed by up to 75% and 85% compared to analog FL and BPSK FL. The 75% gain stems from the fact that, the proposed FL uses digital modulation (i.e., 64 QAM) which can combat channel impairments and misalignments thus reducing the errors incurred by model transmission. The 85% gain stems from the fact that the proposed algorithm uses high-order quantization scheme instead of using one bit to represent each FL parameter so as to reduce quantization errors. Fig. 3 also shows that the convergence speed and the identification accuracy of the proposed AirComp method are very close to the proposed FL over noiseless channels, which illustrates that our proposed method can use digital modulation to significantly reduce transmission errors caused by channel fading and noise. From Fig. 3, we can also see that without using MLP for FL gradient predictions, the proposed method cannot converge. This is because the PS cannot adjust beamforming matrices without knowing the gradient vectors of each device thus introducing demodulation errors.

In Fig. 4, we show how the identification accuracy of all considered algorithms changes as the number of iterations varies for Fashion-MNIST. In this figure, we can see that, the proposed algorithm improves the identification accuracy by up to 10.5% and 20.5% compared to analog FL and BPSK FL, respectively. From Fig. 4, we can also see that analog FL converges to a bad model. This is because the noise over wireless channels introduces dynamic errors into FL

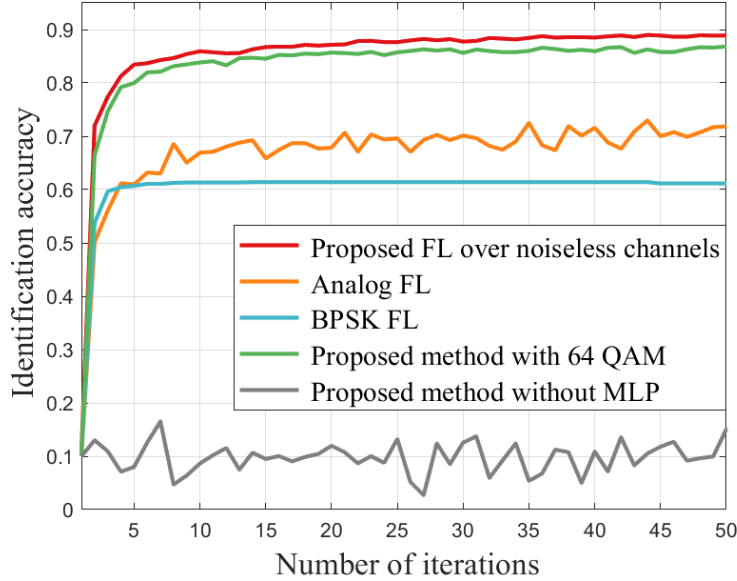


Fig. 4. Identification accuracy vs. number of iterations on Fashion-MNIST dataset.

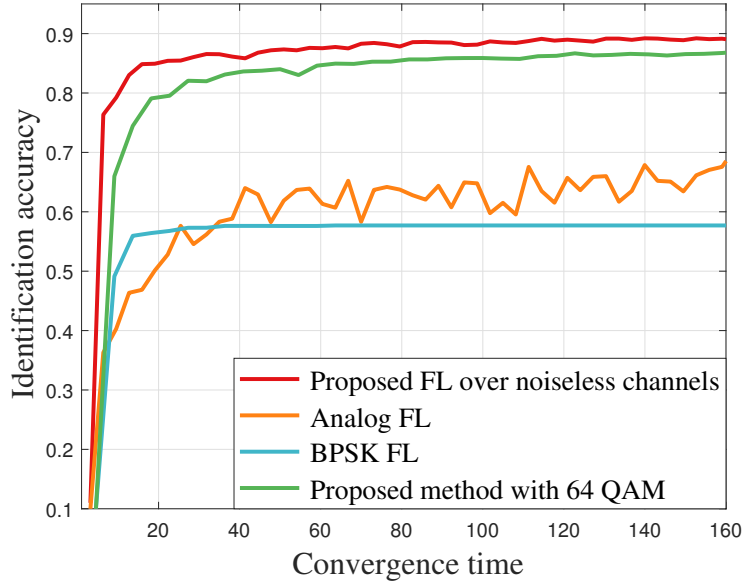


Fig. 5. Identification accuracy vs. convergence time on Fashion-MNIST dataset.

parameter transmission process thus affecting FL identification accuracy. Fig. 4 also shows that the proposed method without using MLP for predicting FL gradients cannot converge, which indicates the optimal beamforming matrices design depends on the prediction of FL gradients.

Fig. 5 shows how the identification accuracy changes as the convergence time varies. Here, the convergence time consists of the model training time that of each device updating its FNN model and the model transmission time. In this figure, we can see that, the proposed FL converges

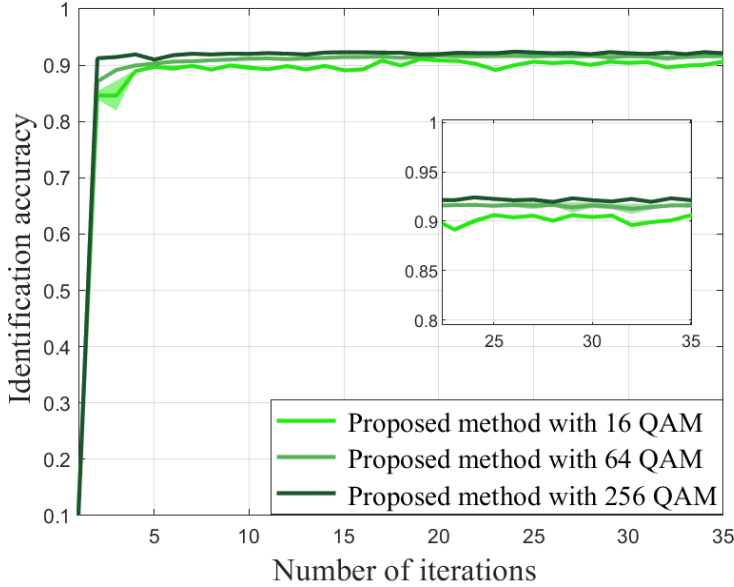


Fig. 6. Identification accuracy vs. number of iterations on MNIST dataset.

slowly but can improve identification accuracy by up to 17% compared to BPSK FL. This is because the proposed FL uses more bits instead of one bit in BPSK FL to represent each FL parameter thus increasing the dynamics of global FL model generation.

In Fig. 6, we show how the identification accuracy of the proposed AirComp methods changes as the modulation order M varies. In this figure, we can see that as M increases, the identification accuracy of the considered algorithms increases. This is due to the fact that, as M increases, each device can use more bits to represent one FL parameter thus reducing quantization errors. However, as M continues to increase, the identification accuracy of the proposed algorithm remains a constant. This is because as M is larger than 64, quantization errors are minimized.

Fig. 7 shows the distribution of the trained FL parameters obtained by the proposed methods as modulation order changes. In this figure, we use different colors to represent the percentage of the trained parameters being a certain value. In particular, as the percentage of the value in trained parameters increases, the color of that value changes from blue to pink. For example, the percentage of the pink block (i.e., +1.5 in BPSK) is 0.7 while the percentage of the cyan block (i.e., -1.5 in BPSK) is 0.3. From Fig. 7, we can see that in BPSK FL, the values of 70% FL parameters in FL model are +1.5 and the values of 30% FL parameters are -1.5. This is because in BPSK FL, each FL weight is represented by 1 bit. Hence, each weight has only two possible values (i.e., +1.5/-1.5). From Fig. 7, we can also see that in the proposed method with

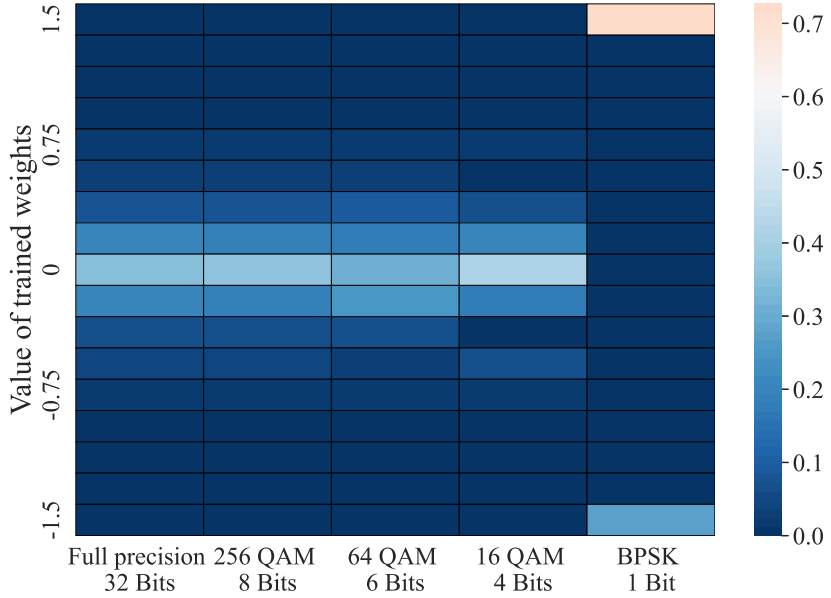


Fig. 7. Distributions of weights for different modulation orders on MNIST dataset.

64 QAM, the values of 30%, 30%, and 20% FL parameters in FL model are 0, -0.375, and +0.375. This is because each FL parameter in the proposed FL with 64 QAM is represented by 6 bits and hence, each FL parameter has 64 possible values which can better approach the full precision FL parameters compared to BPSK FL. Fig. 7 also shows that as the modulation order M increases from 64 to 256, the distribution of the FL parameters are unchanged. This is because using a modulation order M that is larger than 64 cannot further decrease quantization errors and improve identification accuracy of the trained model.

B. Impacts of SNR

In Fig. 8, we show how the identification accuracy changes as SNR decreases. From this figure, we can see that, the identification accuracy decreases as SNR decreases (equivalently noise power increases). This is because as SNR decreases, the probability of incurring transmission error increases, which results in additional errors in FL model training and decreases the FL identification accuracy. Fig. 8 also shows that the proposed AirComp method improves the identification accuracy by up to 15% compared to analog FL when SNR is 15 dB. This is due to the fact that the proposed method can reduce transmission errors introduced by wireless channel noise via digital demodulation. Meanwhile, compared to BPSK FL, the proposed method can achieve up to 10% gain in terms of identification accuracy when SNR is 25 dB. This is because BPSK FL uses one bit to represent each FL parameter thus introducing quantization errors and

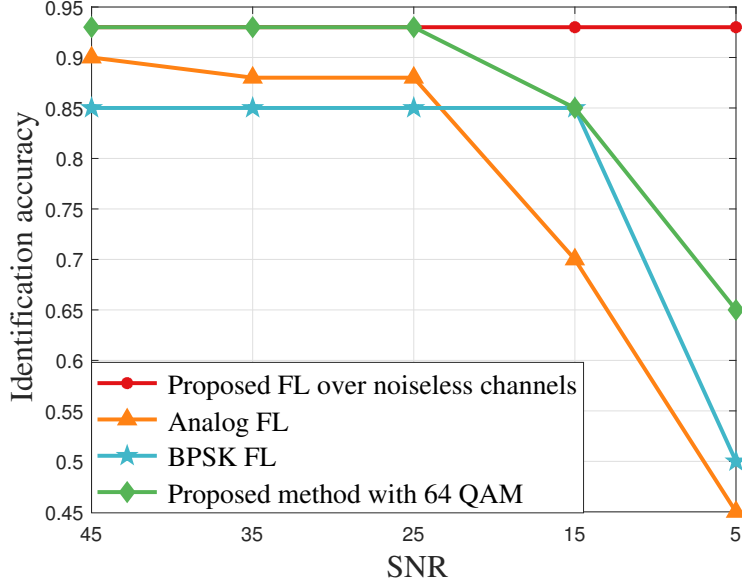


Fig. 8. Identification accuracy vs. SNR on MNIST dataset.

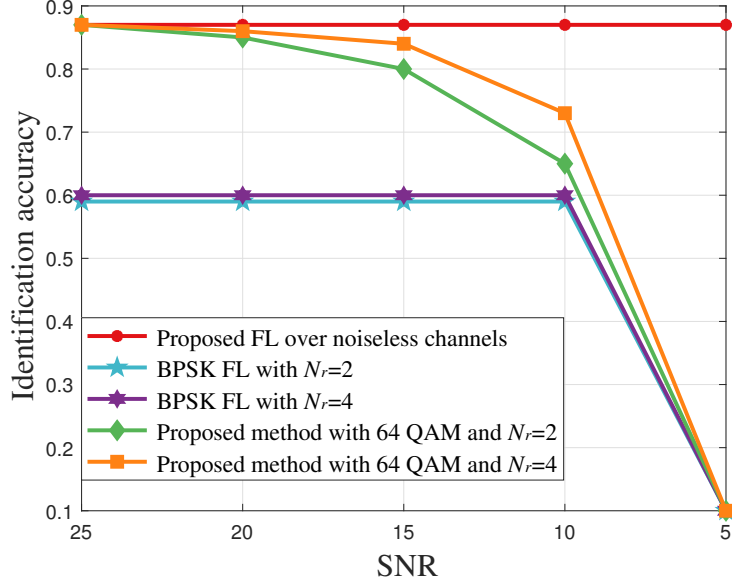


Fig. 9. Identification accuracy vs. SNR on Fashion-MNIST dataset.

decreasing FL performance in terms of identification accuracy. From Fig. 8, we can also see that the identification accuracy of BPSK FL remains a constant as SNR decreases to 15 dB. This is because the decision threshold of BPSK in BPSK FL is larger than that of 64 QAM in the proposed FL. However, as SNR continues to decrease, the identification accuracy of BPSK FL decreases and achieves a 15% accuracy gap compared to the proposed method.

Fig. 9 shows how the identification accuracy of considered FL algorithms changes as SNR

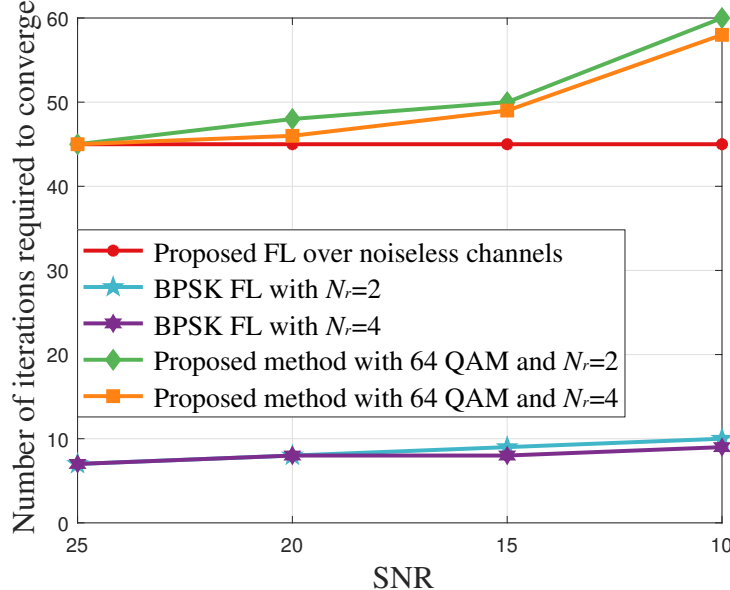


Fig. 10. Number of iterations required to converge vs. SNR on Fashion-MNIST dataset.

decreases. In Fig. 9, we can see that the identification accuracy of the proposed method decreases as SNR decreases while the identification accuracy of BPSK FL remains unchanged as SNR is less than 10 dB. However, the identification accuracy of BPSK FL is lower than the proposed method at any SNR values. This is because the quantization error in BPSK significantly affects the model training process and results in a degeneration of identification accuracy. Fig. 9 also shows that the proposed method with 4 receiver antennas can achieve 8% gains in terms of identification accuracy compared to that with 2 receiver antennas when SNR is 10 dB. This implies that an increase of the number of receiver antennas can improve the identification accuracy in the proposed FL framework. This is because an increase of the number of receiver antennas enables the PS to exploit transmit diversity and reduce transmission error in the AirComp-based system. From Fig. 9, we can also see that as SNR is 5 dB, the identification accuracy of the proposed algorithm and BPSK FL decreases to 0.1.

In Fig. 10, we show how the number of iterations that the considered FL algorithms require to converge changes as SNR decreases. In this figure, we can see that the number of iterations required to converge for all considered algorithms increases as SNR decreases. This is due to the fact that, as SNR decreases, the probability of introducing additional transmission errors increases thus reducing the FL convergence speed.

Fig. 11 shows the cumulative distribution function (CDF) curves of the value of the errors for

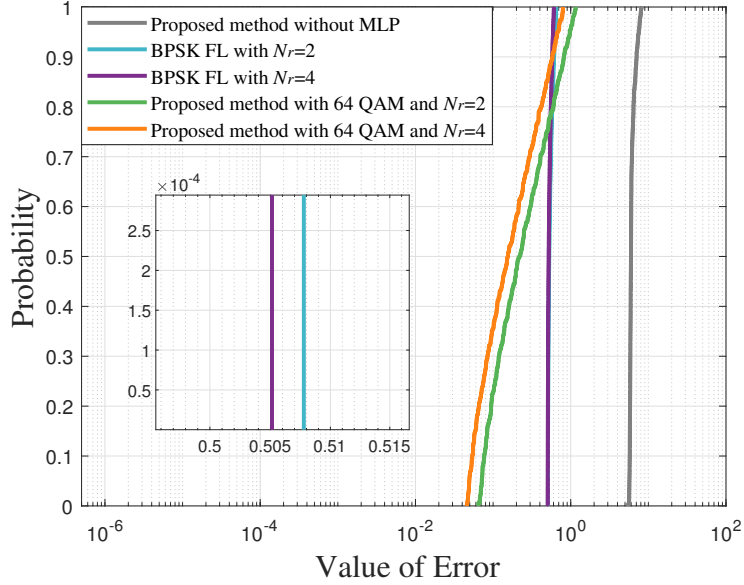


Fig. 11. Cumulative distribution function of value of error on Fashion-MNIST dataset.

all considered algorithms with different number of receiver antennas. The error is defined as the sum of the distances between all weights in the aggregated model and that in the perfect model g_t^* . In Fig. 11, we can see that the proposed method achieves a lower error rate compared to the proposed FL without using MLP for FL gradient prediction. This is because without predicting FL gradient vectors, the PS cannot proactively adjust the transmit and receive beamforming matrices to minimize transmission errors and can only use fixed beamforming design that directly aggregates all local models via linear superimposition. This linear superimposition is not available for digital modulation schemes since digital modulation may introduce complex mapping relationships between bits and symbols thus resulting in additional demodulation errors.

C. Impacts of Network Size

In Fig. 12, we show how the identification accuracy changes as the number of devices varies. From this figure, we can see that, as the number of devices increases, the identification accuracy increases. This is because, as the number of devices that participate in FL training at current iteration increases, the gap between the aggregated model and the perfect model g_t^* at each iteration decreases, thus resulting in a better identification accuracy. Fig. 12 also shows that the proposed method can achieve 3.5% and 7.5% gain in terms of the identification accuracy compared to analog FL and BPSK FL, respectively. This is because the proposed method

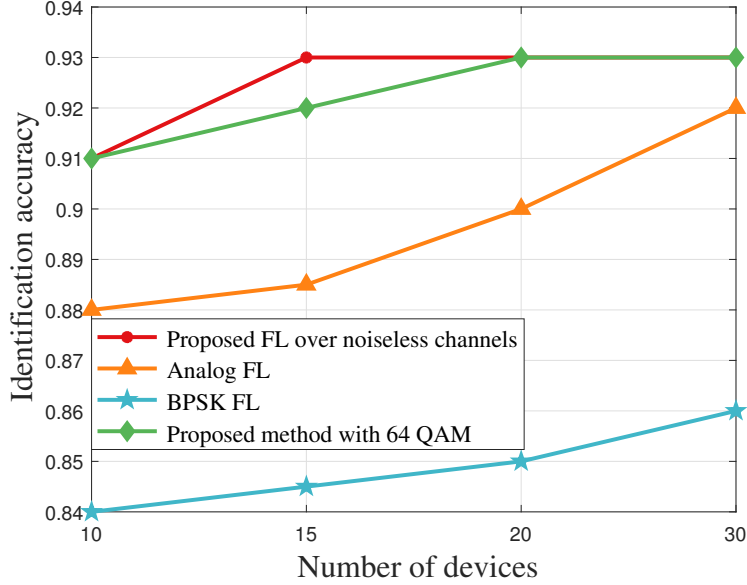


Fig. 12. Identification accuracy vs. number of devices on MNIST dataset.

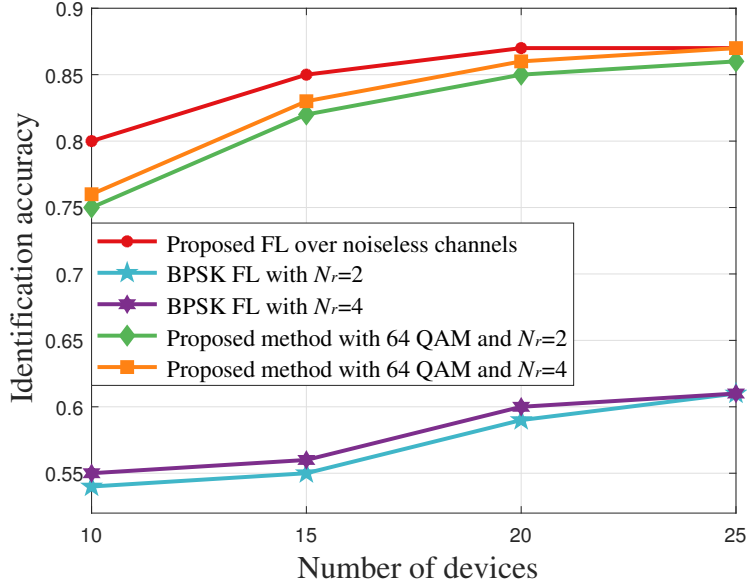


Fig. 13. Identification accuracy vs. number of devices on Fashion-MNIST dataset.

enables the devices to transmit their model parameters using high-order modulation schemes, thus reducing quantization and transmission errors.

Fig. 13 shows how the identification accuracy changes as the number of devices varies. In Fig. 13, we can see that the identification accuracy increases as the number of devices increases. This is because as the number of devices increases, the number of data samples used for training increases, thus resulting in an increase of identification accuracy. From Fig. 13, we see that

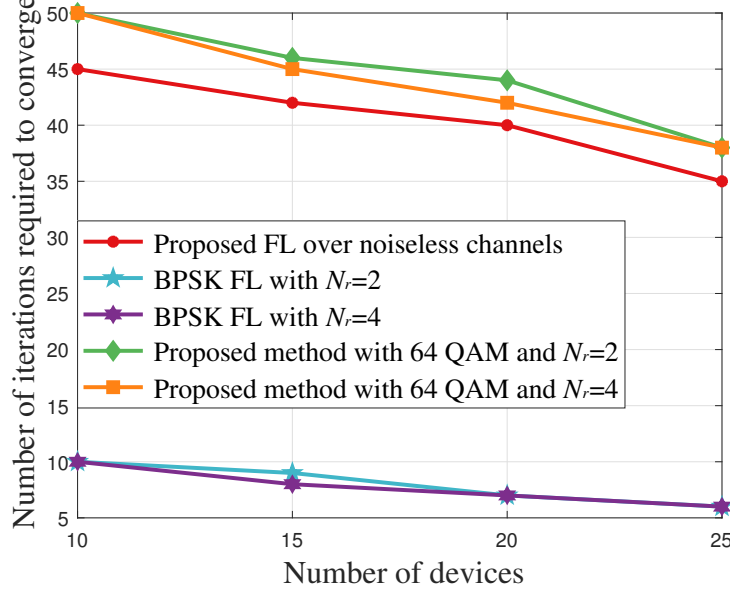


Fig. 14. Number of iterations required to converge vs. number of devices on Fashion-MNIST dataset.

the proposed method can improve 25% identification accuracy compared to baseline BPSK FL. This is because the proposed FL framework enables the PS and the devices to utilize high-order digital modulation to reduce quantization errors. Fig. 13 also shows that as the number of receiver antennas increases, the identification accuracy of the proposed FL remains unchanged. This implies that an increase of the number of receiver antennas may not affect the gain for identification accuracy under ideal channel conditions.

In Fig. 14, we show how the number of iterations required to converge varies as the number of devices changes. From this figure, we can see that, as the number of devices increases, the number of iterations needed to converge decreases. This is because as the number of devices increases, the number of data samples used for training at each FL iteration increases. Fig. 14 also shows that the proposed method can achieve the same performance in terms of convergence speed compared to the proposed FL over noiseless channels, which illustrates that our proposed method can approach perfect model aggregation when considering fading and additive white Gaussian noise.

V. CONCLUSION

In this article, we have developed a novel framework that enables the implementation of FL algorithms over a digital MIMO and AirComp based system. We have formulated an optimization problem that jointly considers transmit and receive beamforming matrices for the minimization

of FL training loss. To solve this problem, we have analyzed the expected improvement of FL training loss between two adjacent iterations that depends on the digital modulation mode, the number of devices, and the design of beamforming matrices. To find the tightest bound, we introduced an ANN based algorithm to estimate the local FL models of all devices and then, the optimal solution of beamforming matrices is determined based on the predicted FL model and the derived expected improvement of FL training loss. Numerical evaluation on real-world machine learning tasks demonstrated that the proposed methodology yields significant gains in classification accuracy and convergence speed compared to conventional approaches.

VI. APPENDIX

A. Proof of Theorem 1

To prove Theorem 1, we first rewrite $F(\mathbf{g}_{t+1})$ using the second-order Taylor expansion and the property of the L -smooth in Assumption a), which can be expressed as

$$F(\mathbf{g}_{t+1}) \leq F(\mathbf{g}_t) + (\mathbf{g}_{t+1} - \mathbf{g}_t) \nabla F(\mathbf{g}_t) + \frac{L}{2} \|\mathbf{g}_{t+1} - \mathbf{g}_t\|^2.$$

Let $\mathbf{g}_{t+1} - \mathbf{g}_t = \nabla F(\mathbf{g}_t) - \mathbf{o}_t$ and the learning rate $\lambda = \frac{1}{L}$, we have

$$\begin{aligned} \mathbb{E}(F(\mathbf{g}_{t+1})) - \mathbb{E}(F(\mathbf{g}_t)) &\leq -\lambda \mathbb{E}(\nabla F(\mathbf{g}_t) - \mathbf{o}_t) \nabla F(\mathbf{g}_t) + \frac{L\lambda^2}{2} \mathbb{E} \|\nabla F(\mathbf{g}_t) - \mathbf{o}_t\|^2 \\ &\stackrel{(a)}{=} -\frac{1}{2L} \mathbb{E} \|\nabla F(\mathbf{g}_t)\|^2 + \frac{1}{2L} \mathbb{E}(\|\mathbf{o}_t\|^2), \end{aligned}$$

where (a) stems from the fact that $\frac{L\lambda^2}{2} \|\nabla F(\mathbf{g}_t) - \mathbf{o}_t\|^2 = \frac{1}{2L} \|\nabla F(\mathbf{g}_t)\|^2 - \frac{1}{L} \mathbf{o}_t^T \nabla F(\mathbf{g}_t) + \frac{1}{2L} \mathbb{E}(\|\mathbf{o}_t\|^2)$ with \mathbf{o}_t being a gradient deviation caused by the errors in local FL model transmission, which can be given as follows

$$\begin{aligned} \mathbb{E}(\|\mathbf{o}_t\|^2) &= \mathbb{E}(\|\nabla F(\mathbf{g}_t) - (\mathbf{g}_{t+1} - \mathbf{g}_t)\|^2) \\ &= \mathbb{E} \left(\left\| \frac{\sum_{k=1}^K \sum_{n=1}^{N_{k,t}} \nabla f(\mathbf{g}_t, \mathbf{x}_{n,k}, \mathbf{y}_{n,k})}{N} - l^{-1} \left(\hat{\mathbf{s}}_t \left(\sum_{n \in \mathcal{N}_{k,t}} \nabla f(\mathbf{g}_t, \mathbf{x}_{n,k}, \mathbf{y}_{n,k}) \right) \right) \right\|^2 \right) \\ &\leq \mathbb{E} \left(\left\| \frac{\sum_{k=1}^K \sum_{n=1}^{N_{k,t}} \nabla f(\mathbf{g}_t, \mathbf{x}_{n,k}, \mathbf{y}_{n,k})}{N} - -l^{-1} \left(\frac{\sum_{k=1}^K l \left(\sum_{n \in \mathcal{N}_{k,t}} \nabla f(\mathbf{g}_t, \mathbf{x}_{n,k}, \mathbf{y}_{n,k}) \right)}{\sum_{k=1}^K |\mathcal{N}_{k,t}|} \right) \right\|^2 \right) \end{aligned}$$

$$+ \left\| l^{-1} \left(\frac{\sum_{k=1}^K l \left(\sum_{n \in \mathcal{N}_{k,t}} \nabla f(\mathbf{g}_t, \mathbf{x}_{n,k}, \mathbf{y}_{n,k}) \right)}{\sum_{k=1}^K |\mathcal{N}_{k,t}|} \right) - l^{-1} \left(\hat{\mathbf{s}}_t \left(\sum_{n \in \mathcal{N}_{k,t}} \nabla f(\mathbf{g}_t, \mathbf{x}_{n,k}, \mathbf{y}_{n,k}) \right) \right) \right\|^2,$$

where $\nabla f(\mathbf{g}_t, \mathbf{x}_{n,k}, \mathbf{y}_{n,k})$ is the gradient trained by $(\mathbf{x}_{n,k}, \mathbf{y}_{n,k})$. $\hat{\mathbf{s}}_t \left(\sum_{n \in \mathcal{N}_{k,t}} \nabla f(\mathbf{g}_t, \mathbf{x}_{n,k}, \mathbf{y}_{n,k}) \right) = \frac{\mathbf{B} \sum_{k=1}^K \mathbf{H}_k \mathbf{A}_k l \left(\sum_{n \in \mathcal{N}_{k,t}} \nabla f(\mathbf{g}_t, \mathbf{x}_{n,k}, \mathbf{y}_{n,k}) \right) + \mathbf{B} \mathbf{n}_t}{\sum_{k=1}^K |\mathcal{N}_{k,t}|}$ is the received signal. $\frac{\sum_{k=1}^K l \left(\sum_{n \in \mathcal{N}_{k,t}} \nabla f(\mathbf{g}_t, \mathbf{x}_{n,k}, \mathbf{y}_{n,k}) \right)}{\sum_{k=1}^K |\mathcal{N}_{k,t}|}$ is the theoretical signal that is obtained via modulation at devices and demodulation at the PS without channel impairments and misalignments.

REFERENCES

- [1] M. Chen, D. Gündüz, K. Huang, W. Saad, M. Bennis, A. V. Feljan, and H. V. Poor, “Distributed learning in wireless networks: Recent progress and future challenges,” *IEEE Journal on Selected Areas in Communications*, vol. 39, no. 12, pp. 3579–3605, Dec. 2021.
- [2] S. Hosseinalipour, C. G. Brinton, V. Aggarwal, H. Dai, and M. Chiang, “From federated to fog learning: Distributed machine learning over heterogeneous wireless networks,” *IEEE Communications Magazine*, vol. 58, no. 12, pp. 41–47, Jan. 2020.
- [3] J. Kang, Z. Xiong, D. Niyato, S. Xie, and J. Zhang, “Incentive mechanism for reliable federated learning: A joint optimization approach to combining reputation and contract theory,” *IEEE Internet of Things Journal*, vol. 6, no. 6, pp. 10700–10714, Dec. 2019.
- [4] D. C. Nguyen, M. Ding, P. N. Pathirana, A. Seneviratne, J. Li, and H. V. Poor, “Federated learning for Internet of Things: A comprehensive survey,” *IEEE Communications Surveys & Tutorials*, vol. 23, no. 3, pp. 1622–1658, April 2021.
- [5] Y. Shen, Y. Qu, C. Dong, F. Zhou, and Q. Wu, “Joint training and resource allocation optimization for federated learning in UAV swarm,” *IEEE Internet of Things Journal*, vol. 10, no. 3, pp. 2272–2284, Feb. 2023.
- [6] X. Wei, C. Shen, J. Yang, and H. V. Poor, “Random orthogonalization for federated learning in massive MIMO systems,” Available Online: <https://arxiv.org/abs/2201.12490>, Jan. 2022.
- [7] W. Guo, R. Li, C. Huang, X. Qin, K. Shen, and W. Zhang, “Joint device selection and power control for wireless federated learning,” *IEEE Journal on Selected Areas in Communications*, vol. 40, no. 8, pp. 2395–2410, Aug. 2022.
- [8] H. Sun, X. Ma, and R. Q. Hu, “Adaptive federated learning with gradient compression in uplink NOMA,” *IEEE Transactions on Vehicular Technology*, vol. 69, no. 12, pp. 16325–16329, Dec. 2020.
- [9] S. Wang, M. Chen, C. G. Brinton, C. Yin, W. Saad, and S. Cui, “Performance optimization for variable bitwidth federated learning in wireless networks,” Available Online: <https://arxiv.org/abs/2209.10200>, Sep. 2022.
- [10] T. Liu, B. Di, S. Wang, and L. Song, “A privacy-preserving incentive mechanism for federated cloud-edge learning,” in *Proc. IEEE Global Communications Conference*, Madrid, Spain, Dec. 2021.
- [11] T. Sery, N. Shlezinger, K. Cohen, and Y. C. Eldar, “Over-the-air federated learning from heterogeneous data,” *IEEE Transactions on Signal Processing*, vol. 69, pp. 3796–3811, June 2021.
- [12] N. Zhang and M. Tao, “Gradient statistics aware power control for over-the-air federated learning,” *IEEE Transactions on Wireless Communications*, vol. 20, no. 8, pp. 5115–5128, March 2021.

- [13] S. Jing and C. Xiao, "Federated learning via over-the-air computation with statistical channel state information," *IEEE Transactions on Wireless Communications*, to appear, 2022.
- [14] W. Ni, Y. Liu, Y. C. Eldar, Z. Yang, and H. Tian, "STAR-RIS integrated nonorthogonal multiple access and over-the-air federated learning: Framework, analysis, and optimization," *IEEE Internet of Things Journal*, vol. 9, no. 18, pp. 17136–17156, Sept. 2022.
- [15] C. Zhong, H. Yang, and X. Yuan, "Over-the-air federated multi-task learning over MIMO multiple access channels," *IEEE Transactions on Wireless Communications*, to appear, 2022.
- [16] Y. Shao, D. Gündüz, and S. C. Liew, "Federated edge learning with misaligned over-the-air computation," *IEEE Transactions on Wireless Communications*, vol. 21, no. 6, pp. 3951–3964, Nov. 2022.
- [17] Z. Wang, Y. Zhou, Y. Shi, and W. Zhuang, "Interference management for over-the-air federated learning in multi-cell wireless networks," *IEEE Journal on Selected Areas in Communications*, vol. 40, no. 8, pp. 2361–2377, June 2022.
- [18] W. Fang, Z. Yu, Y. Jiang, Y. Shi, C. N. Jones, and Y. Zhou, "Communication-efficient stochastic zeroth-order optimization for federated learning," *IEEE Transactions on Signal Processing*, vol. 70, pp. 5058–5073, Oct. 2022.
- [19] X. Ma, H. Sun, Q. Wang, and R. Q. Hu, "User scheduling for federated learning through over-the-air computation," in *Proc. IEEE Vehicular Technology Conference*, Norman, OK, USA, Sept. 2021.
- [20] H. Guo, A. Liu, and V. K. N. Lau, "Analog gradient aggregation for federated learning over wireless networks: Customized design and convergence analysis," *IEEE Internet of Things Journal*, vol. 8, no. 1, pp. 197–210, June 2021.
- [21] M. Huh, D. Yu, and S. H. Park, "Signal processing optimization for federated learning over multi-user MIMO uplink channel," in *Proc. International Conference on Information Networking*, Jeju Island, Korea (South), Jan. 2021.
- [22] Z. Wang, J. Qiu, Y. Zhou, Y. Shi, L. Fu, W. Chen, and K. B. Letaief, "Federated learning via intelligent reflecting surface," *IEEE Transactions on Wireless Communications*, vol. 21, no. 2, pp. 808–822, Feb. 2022.
- [23] C. Xu, S. Liu, Z. Yang, Y. Huang, and K. K. Wong, "Learning rate optimization for federated learning exploiting over-the-air computation," *IEEE Journal on Selected Areas in Communications*, vol. 39, no. 12, pp. 3742–3756, Dec. 2021.
- [24] Y. Hu, M. Chen, M. Chen, Z. Yang, M. Shikh-Bahaei, H. V. Poor, and S. Cui, "Energy minimization for federated learning with IRS-assisted over-the-air computation," in *Proc. IEEE International Conference on Acoustics, Speech and Signal Processing*, Oronto, ON, Canada, June 2021.
- [25] S. Xia, J. Zhu, Y. Yang, Y. Zhou, Y. Shi, and W. Chen, "Fast convergence algorithm for analog federated learning," in *Proc. IEEE International Conference on Communications*, Montreal, QC, Canada, June 2021.
- [26] M. M. Amiri, T. M. Duman, D. Gündüz, S. R. Kulkarni, and H. V. Poor, "Blind federated edge learning," *IEEE Transactions on Wireless Communications*, vol. 20, no. 8, pp. 5129–5143, March 2021.
- [27] H. Liu, X. Yuan, and Y. J. A. Zhang, "CSIT-free model aggregation for federated edge learning via reconfigurable intelligent surface," *IEEE Wireless Communications Letters*, vol. 10, no. 11, pp. 2440–2444, Aug. 2021.
- [28] G. Zhu, Y. Du, D. Gündüz, and K. Huang, "One-bit over-the-air aggregation for communication-efficient federated edge learning: Design and convergence analysis," *IEEE Transactions on Wireless Communications*, vol. 20, no. 3, pp. 2120–2135, Nov. 2021.
- [29] R. Jiang and S. Zhou, "Cluster-based cooperative digital over-the-air aggregation for wireless federated edge learning," in *Proc. IEEE International Conference on Communications in China*, Chongqing, China, Aug. 2020.
- [30] X. Zhao, L. You, R. Cao, Y. Shao, and L. Fu, "Broadband digital over-the-air computation for asynchronous federated edge learning," Available Online: <https://arxiv.org/abs/2111.10508>, Nov. 2021.
- [31] M. M. Amiri and D. Gündüz, "Machine learning at the wireless edge: Distributed stochastic gradient descent over-the-air," *IEEE Transactions on Signal Processing*, vol. 68, pp. 2155–2169, March 2020.

- [32] Z. Lin, X. Li, V. K. N. Lau Y. Gong, and K. Huang, “Deploying federated learning in large-scale cellular networks: Spatial convergence analysis,” *IEEE Transactions on Wireless Communications*, vol. 21, no. 3, pp. 1542–1556, Aug. 2022.
- [33] H. Xing, O. Simeone, and S. Bi, “Federated learning over wireless device-to-device networks: Algorithms and convergence analysis,” *IEEE Journal on Selected Areas in Communications*, vol. 39, no. 12, pp. 3723–3741, Oct. 2021.
- [34] H. Jeddah, A. Mezghani, A. L. Swindlehurst, and J. A. Nossek, “Quantized constant envelope precoding with PSK and QAM signaling,” *IEEE Transactions on Wireless Communications*, vol. 17, no. 12, pp. 8022–8034, Dec. 2018.
- [35] M. Chen, Z. Yang, W. Saad, C. Yin, H. V. Poor, and S. Cui, “A joint learning and communications framework for federated learning over wireless networks,” *IEEE Transactions on Wireless Communications*, vol. 20, no. 1, pp. 269–283, Jan. 2021.
- [36] S. Haykin, *Neural Networks and Learning Machines*, Pearson Education, Cranbury, NJ, USA, 2009.
- [37] S. Boyd and L. Vandenberghe, *Convex Optimization*, Cambridge University Press, Cambridgeshire, UK, 2004.
- [38] S. Wang, M. Chen, X. Liu, C. Yin, S. Cui, and H. Vincent Poor, “A machine learning approach for task and resource allocation in mobile-edge computing-based networks,” *IEEE Internet of Things Journal*, vol. 8, no. 3, pp. 1358–1372, July 2021.
- [39] L. Deng, “The mnist database of handwritten digit images for machine learning research,” *IEEE Signal Processing Magazine*, vol. 29, no. 6, pp. 141–142, Nov. 2012.
- [40] H. Xiao, K. Rasul, and R. Vollgraf, “Fashion-mnist: a novel image dataset for benchmarking machine learning algorithms,” Available Online: <https://arxiv.org/abs/1708.07747>, Aug. 2017.